2019 December 16

Orbital State Covariance Interpolation Using State Transition Matrices

Doyle T. Hall — Omitron, Inc. (with assistance from the CARA Analysis Team)

Introduction

Satellite conjunction risk analysis requires estimates of orbital state vectors and associated covariance matrices.[1] Specifically, calculating a conjunction's collision probability (Pc) using the "2D-Pc" approximation method[2,3] or the "from-TCA Monte Carlo" simulation method[4-6] employs mean high-fidelity states and covariances for both the primary and secondary satellites estimated at their time of closest approach (TCA). Typical satellite trajectory ephemerides, however, contain states and covariances only at discrete times, which do not in general correspond to a conjunction's TCA. Ephemeris-based Pc analysis therefore relies on estimating accurate states and covariances at TCAs that occur between the discrete ephemeris times.[7]

TCA orbital state vectors can usually be estimated sufficiently accurately for conjunction risk analysis using currently-implemented interpolation schemes. However, experience has demonstrated that covariances can be more difficult to interpolate sufficiently accurately.[8] Specifically, applying even advanced multi-point or high-order interpolation schemes directly to ephemeris covariances has been observed to produce interpolant matrices that are non-positive definite (NPD). Because such NPD covariances do not provide physically plausible representations of actual TCA state uncertainty distributions, they could adversely affect the Pc estimation process.

This analysis outlines how conjunction TCA covariances can be estimated from ephemerides using two alternative methods formulated specifically to preclude the production of NPD covariances. Both methods employ state transition matrices (STMs). The first "STM interpolation" approach is the more accurate of the two, but requires ephemerides that contain STMs rather than (or in addition to) covariances. The second "STM-based covariance blending" approach can be applied to ephemerides that only contain covariances, such as those produced by many satellite owner/operators.

Propagated State and Covariance Ephemerides

This section provides a conceptualized overview of ephemerides produced by high-fidelity *Special Perturbations* (SP) propagations computed using the United States Air Force's *Astrodynamics Support Workstation* (ASW) processing system.[9,10] Operational ASW SP ephemerides will soon change in both content and format; this section also provides an overview and justification of these changes.

Orbital Determination Solutions Satellite orbit determination (OD) solutions provide the means to predict trajectories and construct ephemerides. OD solutions consist of an epoch time along with a satellite's probabilistic mean orbital state and associated covariance matrix, $\{t_0, \mathbf{S}_0, \boldsymbol{\mathcal{P}}_0\}$, which are estimated from a combined and weighted set of trajectory metric observations.[11,12] The epoch time t_0 for an SP OD solution usually coincides with the latest metric observation's acquisition time. The mean (or best-estimate) SP orbital state vector $\mathbf{S}_0$ consists of an inertial frame position-velocity vector combined with a vector of auxiliary state variables[11]

$$\mathbf{S}_0 = \mathbf{S}(t_0) = \begin{bmatrix} \mathbf{r}_0 \\ \mathbf{v}_0 \\ \mathbf{m} \end{bmatrix} = \begin{bmatrix} \mathbf{X}_0 \\ \mathbf{m} \end{bmatrix} \tag{1}$$

with $\mathbf{r}_0$ representing the epoch position vector, $\mathbf{v}_0$ the epoch velocity vector, $\mathbf{m}$ a time-invariant vector of auxiliary model parameters, and $\mathbf{X}_0$ the combined position-velocity epoch state vector. Eq. (1) indicates that SP states are expressed as $N_\mathrm{S}\times 1$ column vectors, with dimension $N_\mathrm{S} = 6 + N_\mathrm{m}$. The number and form of the auxiliary variables required for high-fidelity propagation can vary for different satellites (and also for different propagation schemes), but a representative ASW SP state contains two auxiliary model parameters ($N_\mathrm{m} = 2$), and has the form $\mathbf{m} = [B\ R]^T$, with B denoting a ballistic coefficient, and R a solar radiation pressure parameter. The actual epoch state for a satellite differs from the mean state because of measurement and modeling uncertainties, $\mathbf{S}_0 = \mathbf{S}_{0,\mathrm{actual}} + \mathbf{s}_0$, and the OD process also provides an estimate of the $N_\mathrm{S}\times N_\mathrm{S}$ covariance matrix, $\boldsymbol{\mathcal{P}}_0 = E[\mathbf{s}_0\mathbf{s}_0^T]$, which represents the expected value of the outer vector product $\mathbf{s}_0\mathbf{s}_0^T$. Properly formulated and realistically implemented OD solutions (such as those provided by the ASW system) provide epoch covariances with two essential qualities: each $\boldsymbol{\mathcal{P}}_0$ matrix is both symmetric and positive definite.[12]

Satellite Ephemerides SP ephemerides currently contain states and covariances propagated from the OD epoch time to a set of discrete times $\{t_j\}$. These times increase monotonically (i.e., $t_j < t_{j+1}$), but are not necessarily evenly spaced. Propagated SP ephemeris states $\mathbf{S}_j = \mathbf{S}(t_j)$ are calculated from the OD analysis solution using high-fidelity multivariate numerical integration. Propagating the covariance entails applying a state transition matrix (STM) as follows[11,12]

$$\boldsymbol{\mathcal{P}}_j = \boldsymbol{\mathcal{P}}(t_j) = \boldsymbol{\Phi}_j\, \boldsymbol{\mathcal{P}}_0\, \boldsymbol{\Phi}_j^T \tag{2}$$

Here $\boldsymbol{\Phi}_j$ denotes the STM for ephemeris time t_j, which represents an $N_\mathrm{S}\times N_\mathrm{S}$ matrix of partial derivatives

$$\boldsymbol{\Phi}_j = \boldsymbol{\Phi}(t_j, t_0) = \frac{\partial \mathbf{S}_j}{\partial \mathbf{S}_0} \tag{3}$$

As mentioned previously, a proper OD solution provides an epoch covariance matrix $\boldsymbol{\mathcal{P}}_0$ that is both symmetric and positive definite. Propagating covariances using eq. (2) preserves these qualities to within computational round-off error precision limits, as long as the STM $\boldsymbol{\Phi}_j$ has full rank.

An SP ephemeris state covariance matrix can each be decomposed into six sub-matrices as follows

$$\boldsymbol{\mathcal{P}}_j = \begin{bmatrix} \mathbf{A}_j & \mathbf{B}_j^T & \mathbf{D}_j^T \\ \mathbf{B}_j & \mathbf{C}_j & \mathbf{E}_j^T \\ \mathbf{D}_j & \mathbf{E}_j & \mathbf{F}_j \end{bmatrix} \tag{4}$$

with $\mathbf{A}_j$ representing the marginalized 3×3 covariance of the position vector, $\mathbf{C}_j$ the marginalized 3×3 covariance of the velocity vector, $\mathbf{F}_j$ the marginalized $N_\mathrm{m}\times N_\mathrm{m}$ covariance of the auxiliary vector, and the three remaining matrices $(\mathbf{B}_j, \mathbf{D}_j, \mathbf{E}_j)$ representing cross correlations.

As mentioned previously, ASW SP ephemerides will soon change. Before the change, an SP ephemeris could be represented conceptually as the combined set of discrete times, states and associated covariances: $\{t_j, \mathbf{S}_j, \boldsymbol{\mathcal{P}}_j\}$. This form will be replaced with a new version that enables STM-based estimations of conjunction covariances. This new SP ephemeris table can be conceptually represented by the combined set $\{t_0, \mathbf{S}_0, \boldsymbol{\mathcal{P}}_0;\ t_j, \mathbf{S}_j, \boldsymbol{\Phi}_j\}$, which differs in two ways from the previous version. First, it now explicitly includes the OD solution quantities $\{t_0, \mathbf{S}_0, \boldsymbol{\mathcal{P}}_0\}$, stored in a table header. Second, the new time-ordered table $\{t_j, \mathbf{S}_j, \boldsymbol{\Phi}_j\}$ contains the STM matrices $\boldsymbol{\Phi}_j$ instead of the covariances $\boldsymbol{\mathcal{P}}_j$; the latter

can be calculated using eq. (2) as required. (Note, these conceptual ephemeris representations differ in several respects from actual ASW SP ephemerides. For instance, the old version actually tabulates only the non-redundant elements of the symmetric covariances. Also, rather than tabulating the full $N_S \times N_S$ $\mathbf{\Phi}_j$ matrices, the new version only contains $6 \times N_S$ STM submatrices that are minimally sufficient for conjunction covariance computation, as explained below.)

Position-Velocity Orbital State Vectors and Covariances The position-velocity state for ephemeris time t_j can be extracted from the tabulated full SP state

$$\mathbf{X}_j = \begin{bmatrix} \mathbf{r}_j \\ \mathbf{v}_j \end{bmatrix} \tag{5}$$

The marginalized 6×6 covariance matrix for this position-velocity state is given by the upper-left portion of the full SP state covariance matrix in eq. (4), and can also be propagated from the epoch covariance using an STM

$$\mathbf{P}_j = \begin{bmatrix} \mathbf{A}_j & \mathbf{B}_j^T \\ \mathbf{B}_j & \mathbf{C}_j \end{bmatrix} = \mathbf{\Psi}_j \, \boldsymbol{\mathcal{P}}_0 \, \mathbf{\Psi}_j^T \tag{6}$$

with $\mathbf{\Psi}_j$ representing the upper $6 \times N_S$ sub-matrix of $\mathbf{\Phi}_j$. (Note: The STM $\mathbf{\Psi}_j$ in eq. (6) transforms an OD epoch cartesian-based SP state covariance, $\boldsymbol{\mathcal{P}}_0$, into an inertial frame position-velocity state covariance, $\mathbf{P}_j$. However, for storage and computational efficiency, the new-format ASW SP ephemerides actually tabulate $6 \times N_S$ STMs that transform an OD epoch equinoctial element-based SP state covariance into radial-transverse-normal reference frame position-velocity covariances.)

Equinoctial Element Orbital State Vectors and Covariances Position-velocity states can be transformed into equinoctial orbital element states numerically using a nonlinear conversion method.[13-15] The mean equinoctial state at ephemeris time t_j can be represented by the 6×1 vector

$$\mathbf{Y}_j = \mathbf{Y}(t_j) = \begin{bmatrix} n \\ a_f \\ a_g \\ \chi \\ \psi \\ \lambda_M \end{bmatrix}_{t=t_j} \tag{7}$$

(see references 14 and 15 for further details on these equinoctial elements, which are listed in a different order and with slightly different notation than that used for operational SP processing). The equinoctial state covariance can be calculated using a 6×6 transformation matrix of partial derivatives[15]

$$\mathbf{Q}_j = \mathbf{M}_j \, \mathbf{P}_j \, \mathbf{M}_j^T \qquad \text{with} \qquad \mathbf{M}_j = \frac{\partial \mathbf{Y}_j}{\partial \mathbf{X}_j} \tag{8}$$

Again, when properly formulated and implemented, the transformation in eq. (8) preserves the symmetry and positive definiteness of covariance matrices, to within computational precision limits.

Conjunction TCA Covariances Required for Collision Probability Estimation

The ephemeris covariance matrices described in the previous section represent orbital state uncertainties at the discrete times $\{t_j\}$. Collision probability estimation, however, requires covariances

for the primary and secondary satellites estimated at a conjunction's TCA, which generally does not coincide with any of these ephemeris times. Interpolating ephemeris covariances directly (as the ASW system currently does) can provide the required TCA covariance estimates, but this approach has been observed to produce NPD matrices, even when using advanced interpolation schemes.[8]

Specifically, collision probability estimation using the 2D-Pc method requires inertial frame position covariances at a conjunction's TCA for both the primary and secondary satellites.[1-3] This requires estimating the 3×3 position covariance $\mathbf{A} = \mathbf{A}(t = \mathrm{TCA})$ from the ephemeris for each object. Analysis of archived conjunctions has demonstrated that applying advanced interpolation schemes directly to the relevant set of bracketing ephemeris covariances $\{\mathbf{A}_k\}$ occasionally produces an NPD interpolant matrix $\mathbf{A}$, with a notably larger NPD occurrence frequency for high-eccentricity orbits.[8] This NPD covariance production occurs despite the fact that, in typical circumstances, all of the bracketing covariances $\{\mathbf{A}_k\}$ are positive definite. (For reference, linear or first-order interpolation schemes use two bracketing points that bound the TCA time. Advanced multi-point schemes add additional bracketing points to produce a more accurate, higher-order estimate for the interpolant. Other advanced schemes[7] add first and second derivative information to reduce interpolation errors.)

Pc estimation using "two-body motion from TCA" Monte Carlo (TBMC-Pc) simulations requires the equinoctial state covariance matrix $\mathbf{Q} = \mathbf{Q}(t = \mathrm{TCA})$ for both the primary and secondary satellites.[6] Archive analysis has demonstrated that direct interpolation of 6×6 ephemeris covariances such as $\mathbf{Q}_j$ (or $\mathbf{P}_j$) also creates NPD interpolants—again, more frequently for high-eccentricity orbits, and also with a much higher overall frequency than observed for 3×3 position matrices.[8]

NPD Covariance Production Resulting from SP Ephemeris Covariance Interpolation

As ephemeris propagation time intervals $t_j - t_0$ grow, the covariances $\mathbf{A}_j$, $\mathbf{P}_j$, and $\mathbf{Q}_j$ (and their associated correlation matrices) tend to become more poorly conditioned, i.e., their matrix condition numbers tend to increase with propagation time. Condition numbers also tend to become significantly larger near perigee for high-eccentricity orbits. Introducing small perturbations (such as interpolation inaccuracies, or even computational round-off errors) into a very poorly conditioned covariance can transform it from a positive definite matrix into an NPD matrix. This is why covariances are susceptible to becoming NPD when interpolated directly, especially for long propagations and eccentric orbits, prompting the development of alternative methods designed specifically to preclude NPD covariances.

Figure 1 provides an illustration of how applying advanced multi-point or high-order interpolation schemes can produce NPD covariances. This example employs a 5-day ASW SP ephemeris for a defunct rocket-body (SCN 41195) in a high-eccentricity orbit ($e \approx 0.63$) with a low perigee altitude ($h_p \approx 150\ \mathrm{km}$), containing 13,766 discrete times with spacing that varies between 7.7 s and 72.5 s. This specific SP ephemeris has been found to be especially challenging with respect to NPD covariance production from interpolation. The analyses presented in Figure 1 apply two different interpolation schemes implemented in the Matlab programming language to calculate interpolated estimates, $\mathbf{P}_j^I$, for the ephemeris covariances themselves, $\mathbf{P}_j$. (Both of these interpolation analyses estimate the interpolant $\mathbf{P}_j^I$ using the appropriate set of bracketing points that, of course, does not include the original tabulated covariance estimate, $\mathbf{P}_j$.) The results can be used to gauge and compare each interpolation scheme's accuracy, and frequency of NPD matrix production.

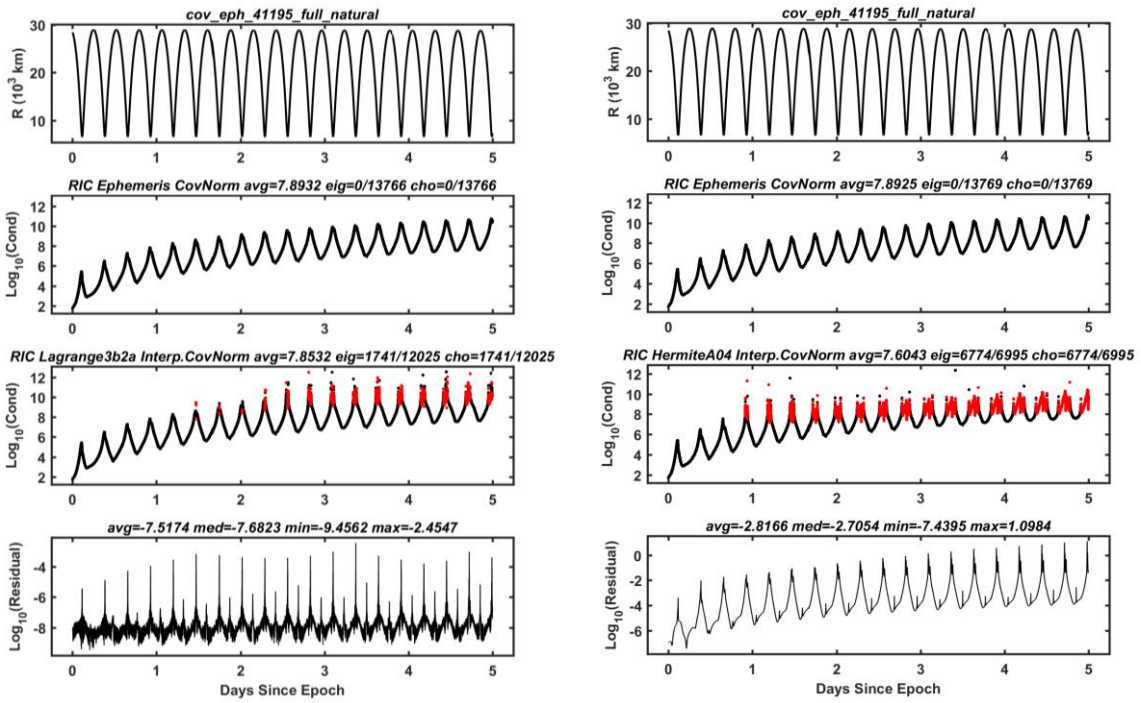

Figure 1. Covariance interpolation of an SP ephemeris for a high-eccentricity orbit using Lagrange 5-point interpolation (left) and Hermite quintic spline interpolation (right).

NPD Production for 5-Point Lagrange Interpolation The left panel in Figure 1 uses a series of four plots to illustrate the effects of applying 5-point Lagrange interpolation. The first graph at the top of the left panel shows the ephemeris radial distances $|\mathbf{r}_j|$ plotted as a function of time. The second graph from the top plots the logarithm of the matrix condition number of the ephemeris position-velocity covariance correlation matrices, indicating an overall increasing trend in time with superimposed peaks that occur at perigee. These ephemeris correlation matrices, $\mathbf{p}_j$, can be calculated from the covariance matrices, $\mathbf{P}_j$, using the following transformation[8]

$$\mathbf{p}_j = \mathbf{D}_j \mathbf{P}_j \mathbf{D}_j \tag{9}$$

where $\mathbf{D}_j$ denotes a diagonal matrix with elements $[\mathbf{D}_j]_{n,m} = \delta_{n,m}/\sqrt{[\mathbf{P}_j]_{n,n}}$ and $\delta_{n,m}$ denotes the Kronecker delta function. The third graph from the top plots the condition number for the interpolant covariances normalized using the same diagonal matrix $\mathbf{D}_j$ as follows: $\mathbf{p}_j^I = \mathbf{D}_j \mathbf{P}_j^I \mathbf{D}_j$. This plot, and the one above, also highlights any detected NPD matrices using red dots, as discussed in more detail below. The bottom-left graph of Figure 1 plots an indicator of the relative differences between the two normalized matrices[16]

$$Residual_j = \frac{\left\| \mathbf{p}_j - \mathbf{p}_j^I \right\|}{\left\| \mathbf{p}_j \right\|} \tag{10}$$

with $\left\| \mathbf{p}_j \right\|$ denoting the Frobenius norm of the matrix $\mathbf{p}_j$. The median residual is about $10^{-7.7}$, meaning that the interpolants $\mathbf{p}_j^I$ from this 5-point Lagrange scheme have a median accuracy about seven to eight decimal places for this ephemeris.[16] At perigee times near the end of the 5-day ephemeris, these residuals grow to ~$10^{-2.5}$ meaning that the associated interpolants can degrade to an accuracy of only two to three decimal places. As mentioned previously, the two middle graphs highlight any NPD

occurrences using red dots. Notably, the second graph from the top has no red dots, indicating no NPD detections among the original 13,766 ephemeris covariances. However, the third graph indicates NPD detections for a significant number (1,741) of the interpolants, which occur predominantly at or near perigee times, and increase in frequency during the 5-day propagation.

NPD Production for Quintic Spline Hermite Interpolation The right panel of Figure 1 uses the same format to show the results of applying a 5th order spline interpolation scheme, designed specifically for orbital states and covariances.[7] The bottom right plot in Figure 1 shows a median residual level of about $10^{-2.7}$, indicating that this scheme produces interpolants with a median accuracy of about two to three decimal places; residuals near perigee times are much larger. The numerous red dots in the panel above also indicate a higher production of NPD matrices than for the Lagrange interpolation scheme (6,774 vs 1,741). Several other interpolation schemes (e.g., cubic spline) applied directly to the covariances also produce NPD interpolants for this challenging SP ephemeris, as well as for many other ephemerides.

Estimating Conjunction TCA Covariances Using STM Interpolation

As mentioned previously, propagating a positive definite covariance using a full-rank STM ensures that the resulting covariance matrix will not be NPD (to within computational precision limits). Accurately estimating a full-rank STM for a conjunction's close approach time, $\mathbf{\Phi} = \mathbf{\Phi}(t = \mathrm{TCA})$, would therefore naturally provide a means of estimating the associated SP state covariance at TCA using the equation

$$\boldsymbol{\mathcal{P}} = \mathbf{\Phi}\, \boldsymbol{\mathcal{P}}_0\, \mathbf{\Phi}^T \tag{11}$$

To accomplish this, the matrix $\mathbf{\Phi}$ itself can be interpolated from a set of bracketing ephemeris matrices $\{\mathbf{\Phi}_k\}$ using an advanced scheme, such as 5-point Lagrange interpolation. This "STM interpolation" approach has the advantage of being much less sensitive to interpolation inaccuracies than the "direct covariance interpolation" approach discussed in the previous section. As long as the interpolant STM $\mathbf{\Phi}$ possesses full rank (which the bracketing matrices $\mathbf{\Phi}_k$ have by construction), then the resultant estimate for the SP state covariance $\boldsymbol{\mathcal{P}}$ produced by eq. (11) will be positive definite (to within computational precision). Furthermore, all of the marginalized and derived sub-matrices of $\boldsymbol{\mathcal{P}}$ will also be positive definite, including the covariances $\mathbf{A}$ and $\mathbf{Q}$ required for collision probability estimation using the 2D-Pc and TBMC-Pc methods, respectively.

The principal advantage of using this STM interpolation method is that it provides full SP state covariances estimated at conjunction TCA times, achieving accuracies comparable to or better than those provided by direct covariance interpolation, but avoids the production of NPD matrices by design. The main disadvantage is that it requires the use of an OD and propagation processing system that is capable of producing and tabulating the appropriate ephemeris STMs. This capability has been recently implemented in the ASW SP processing software. Figure 2 compares the performance of the ASW system before and after these changes, using the same challenging high-eccentricity SP ephemeris discussed previously. The left panel of Figure 2 shows the application of ASW's direct covariance interpolation scheme, which applies a multi-point Lagrange method directly to the ephemeris covariance matrices, and has operated as the default software option for many years. For this ephemeris, ASW's direct covariance interpolation approach produces 2,599 NPD matrices among the 13,769 interpolants, as can be seen in the third plot from the top in the left panel. The panel on the right shows the application of ASW's newly-implemented STM interpolation scheme, which applies multi-point Lagrange interpolation to the appropriate state transition matrices rather than to the covariances.

This approach produces no NPD matrices, as can be seen in the third plot of the right panel. Furthermore, comparing the two bottom plots indicates that the STM interpolation approach also produces systematically smaller residuals than the covariance interpolation approach. This means that, for this ephemeris, the newly implemented approach also yields better interpolation accuracy.

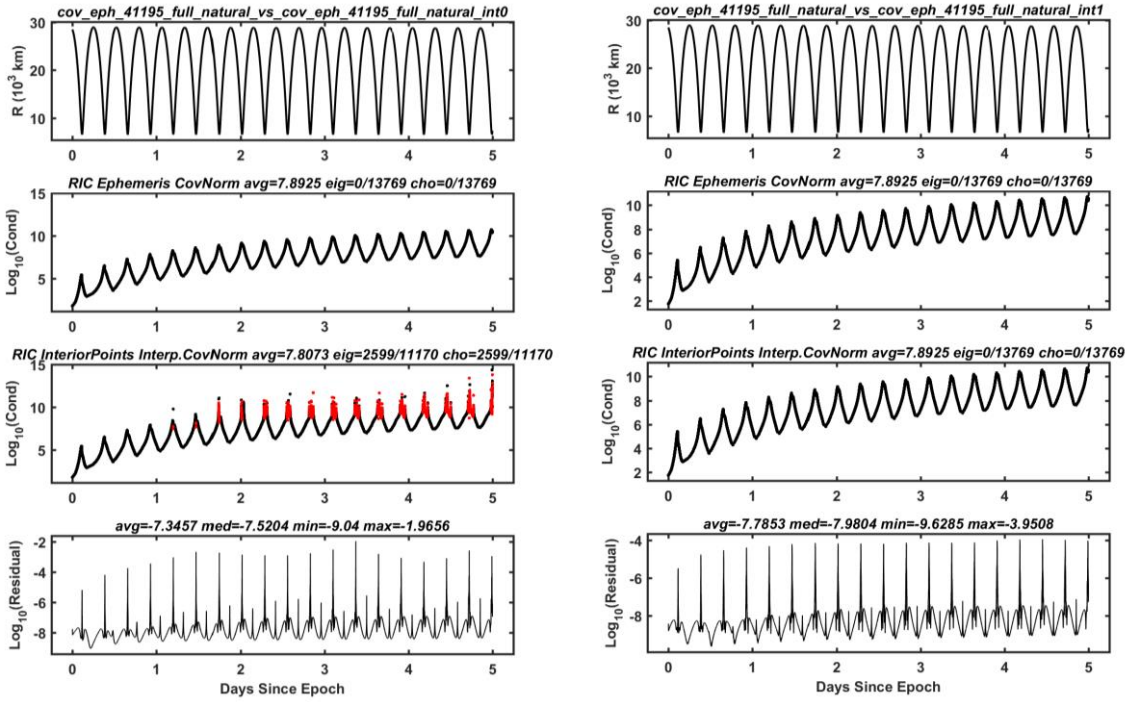

Figure 2. Covariance interpolation of the high-eccentricity SP ephemeris using the ASW system's currently-operational "direct covariance interpolation" scheme (left) and the ASW system's newly-implemented "STM interpolation" scheme (right).

Estimating Conjunction TCA Covariances Using STM-based Covariance Blending

Some ephemerides, such as those produced by satellite owner/operators, will continue to tabulate covariances rather than STMs, preventing the application of the STM interpolation approach presented in the previous section. A typical owner/operator ephemeris can be conceptually represented using the set $\{t_j, \mathbf{X}_j, \mathbf{P}_j\}$, which tabulates inertial frame position-velocity states and covariances. Again, analysis has shown that directly interpolating the $\mathbf{P}_j$ covariances (or the related $\mathbf{A}_j$ and $\mathbf{Q}_j$ covariances) produces undesired NPD interpolants, compelling the development of an alternate approach. This section presents an "STM-based covariance blending" method of estimating conjunction TCA covariances from such owner/operator ephemerides. This approach employs STMs formulated for Keplerian two-body motion[11,17] to propagate ephemeris covariances from both the leading and trailing bracketing ephemeris points, and blends the weighted results, as described below.

<u>STM-based Covariance Blending for Position-Velocity Covariances</u> The position-velocity state covariance, $\mathbf{P} = \mathbf{P}(t)$, for a time t (such as a conjunction TCA) that falls within the span of an ephemeris can be approximated using a four step process. The first step entails finding the sequential pair of ephemeris times (t_k, t_{k+1}) that bracket the time of interest, ensuring that $t_k \leq t \leq t_{k+1}$. The second and third

steps entail calculating the two-body motion STMs that propagate the position-velocity covariance forward in time from the leading bracketing point and backward from the trailing point, as follows

$$\mathbf{P}' = [\boldsymbol{\varphi}(t, t_k)]\ \mathbf{P}_k\ [\boldsymbol{\varphi}(t, t_k)]^T \qquad \text{and} \qquad \mathbf{P}'' = [\boldsymbol{\varphi}(t, t_{k+1})]\ \mathbf{P}_{k+1}\ [\boldsymbol{\varphi}(t, t_{k+1})]^T \tag{12}$$

Here $\boldsymbol{\varphi}(t_b, t_a)$ denotes the two-body motion STM that propagates position-velocity covariances to time t_b from time t_a, as formulated in detail by Shepperd.[17] The fourth and final step entails blending these two results together as a weighted sum, with weighting based on separations from the bracketing ephemeris times, yielding the final approximation

$$\mathbf{P}(t) \approx \mathbf{P}^B(t) = (1 - w)\mathbf{P}' + w\ \mathbf{P}'' \qquad \text{with} \qquad w = (t - t_k)/(\ t_{k+1} - t_k) \tag{13}$$

with the superscript B indicating the blending approximation. Because w and $1 - w$ are both greater or equal to zero, equations (12) and (13) cannot create an NPD matrix (to within computational precision). These two equations also imply that the blending approximation becomes perfectly accurate in the limit that the time of interest coincides with one of the bracketing ephemeris times:

$$\lim_{t \to t_k} \mathbf{P}^B(t) = \mathbf{P}_k \qquad \text{and} \qquad \lim_{t \to t_{k+1}} \mathbf{P}^B(t) = \mathbf{P}_{k+1} \tag{14}$$

For intervening times, eq. (13) yields an approximation that relies on the fact that the bracketing interval $t_{k+1} - t_k$ is sufficiently short that the two-body motion STM provides a reasonably accurate covariance propagation approximation, despite the fact that orbital perturbations are neglected.

STM-based Covariance Blending for Equinoctial Element Covariances An equinoctial orbital element state covariance, $\mathbf{Q} = \mathbf{Q}(t)$, can be approximated using a similar four step blending approach, with the forward and backward propagated covariances given by

$$\mathbf{Q}' = [\boldsymbol{\phi}(t, t_k)]\ \mathbf{Q}_k\ [\boldsymbol{\phi}(t, t_k)]^T \qquad \text{and} \qquad \mathbf{Q}'' = [\boldsymbol{\phi}(t, t_{k+1})]\ \mathbf{Q}_{k+1}\ [\boldsymbol{\phi}(t, t_{k+1})]^T \tag{15}$$

Here $\boldsymbol{\phi}(t_b, t_a)$ denotes the two-body motion STM for equinoctial covariances, which has a relatively simple form with only one nonzero off-diagonal element[11]

$$\boldsymbol{\phi}(t_b, t_a) = \frac{\partial \mathbf{Y}(t_b)}{\partial \mathbf{Y}(t_a)} = \begin{bmatrix} 1 & 0 & 0 & 0 & 0 & 0 \\ 0 & 1 & 0 & 0 & 0 & 0 \\ 0 & 0 & 1 & 0 & 0 & 0 \\ 0 & 0 & 0 & 1 & 0 & 0 \\ 0 & 0 & 0 & 0 & 1 & 0 \\ t_b - t_a & 0 & 0 & 0 & 0 & 1 \end{bmatrix} \tag{16}$$

The blended approximation for $\mathbf{Q}(t)$ is given by

$$\mathbf{Q}(t) \approx \mathbf{Q}^B(t) = (1 - w)\mathbf{Q}' + w\ \mathbf{Q}'' \qquad \text{with} \qquad w = (t - t_k)/(\ t_{k+1} - t_k) \tag{17}$$

Notably this blended equinoctial covariance can then be used to estimate the corresponding position-velocity covariance $\mathbf{P}(t)$ using a transformation[15] similar to eq. (8)

$$\mathbf{P}(t) \approx\ \boldsymbol{\mathcal{M}}[\mathbf{Q}^B(t)]\boldsymbol{\mathcal{M}}^T \qquad \text{with} \qquad \boldsymbol{\mathcal{M}} = \frac{\partial \mathbf{X}(t)}{\partial \mathbf{Y}(t)} \tag{18}$$

The main advantage of using eq. (18) to estimate $\mathbf{P}(t)$, rather than eq. (13), is that it eliminates the need to encode Shepperd's[17] relatively complicated position-velocity STM $\boldsymbol{\varphi}(t_b, t_a)$ into software; the STM $\boldsymbol{\phi}(t_b, t_a)$ given by eq. (16) is much simpler. Two disadvantages are that the transformation matrix $\boldsymbol{\mathcal{M}}$

must be encoded into software (if not already available), and that this method can potentially be less computationally efficient as it may require several otherwise unneeded conversions between position-velocity and equinoctial state/covariance representations. The ASW system implements STM-based covariance blending in equinoctial elements using an approach similar to that outlined in eqs. (15)-(18).

STM-based Covariance Blending Applied to an SP Ephemeris The STM-based blending approach provides a means of effective covariance interpolation that can be applied to an owner/operator ephemeris without producing NPD covariances, to within computational precision limits. Figure 3 demonstrates this by applying this method to the challenging SP ephemeris discussed earlier, acting as if it were a more restricted owner/operator ephemeris. The left panel of Figure 3 shows the results of applying the STM-based blending method as implemented within the ASW system's software. The right panel of Figure 3 shows the results of applying the method as implemented separately within Matlab software. The numerical results are almost identical, meaning that these two implementations of the STM-based covariance blending algorithm produce equivalent results, which provides a measure of cross checking and numerical validation for these two completely independent software implementations.

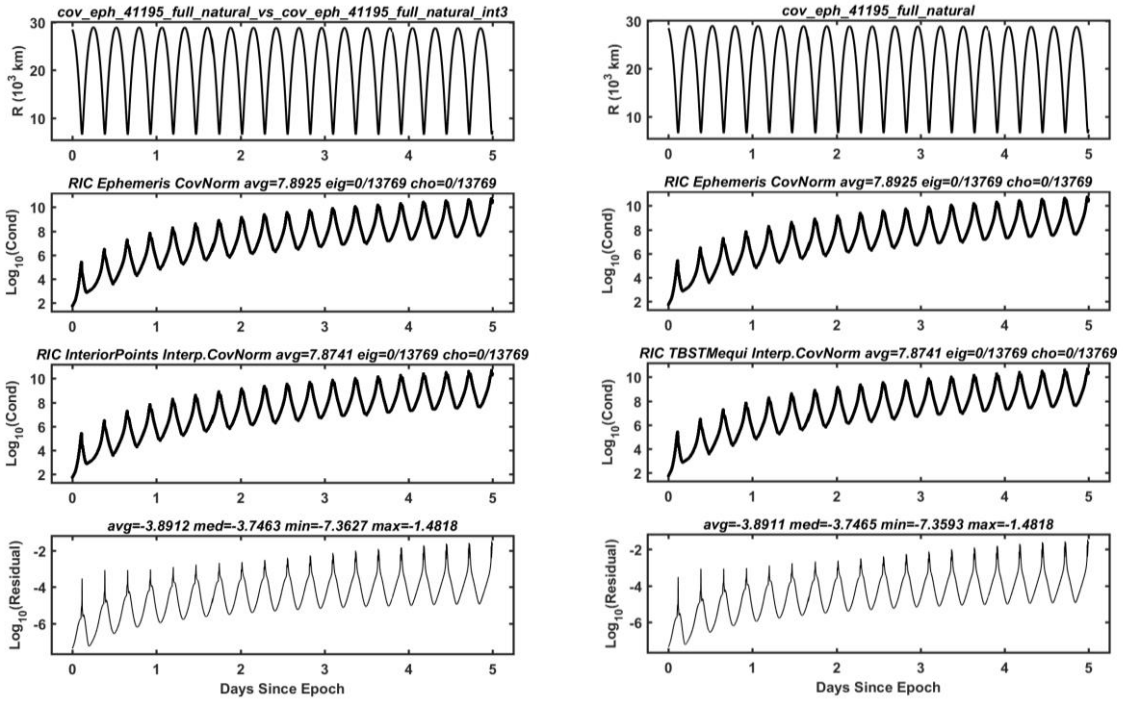

Figure 3. STM-based covariance blending interpolation of the high-eccentricity SP ephemeris using the ASW system's newly-implemented software (left) and an independent Matlab implementation (right).

The bottom graphs in Figure 3 indicate a median residual level of about $10^{-3.7}$ indicating that the STM-based blending method produces interpolants accurate to about three to four decimal places for this ephemeris. Notably, the third graphs from the top in both panels contain no red dots at all, indicating that neither software implementation produced any NPD covariances, also as one would expect, because the STM-based covariance blending method was designed expressly for this purpose.

Covariance Blending Using More Advanced STM Formulations The STM-based covariance blending method could be used with more advanced STMs. For instance, STMs that incorporate the

perturbations from Earth's oblateness through the J_2 gravitational term[18,19] or other effects such as third-body gravitation or atmospheric drag[11,13,20] could potentially improve the accuracy of the method, especially for ephemerides that have long time intervals between tabulated points.

References

[1] K. Chan, *Spacecraft Collision Probability*, El Segundo, CA, The AeroSpace Corporation, 2008.

[2] J.L. Foster and H.S. Estes, "A Parametric Analysis of Orbital Debris Collision Probability and Maneuver Rate for Space Vehicles," NASA/JSC-25898, Aug. 1992.

[3] M.R. Akella and K.T. Alfriend, "The Probability of Collision Between Space Objects," *Journal of Guidance, Control, and Dynamics*, Vol. 23, No. 5, pp. 769-772, 2000.

[4] S. Alfano, "Satellite Conjunction Monte Carlo Analysis," *AAS SpaceFlight Mechanics Meeting*, Pittsburgh, PA, Paper 09-233, Feb. 2009.

[5] C. Sabol, T. Sukut, K. Hill, K. Alfriend, B. Write, Y. Li, and P. Schumacher, "Linearized Orbit Covariance Generation and Propagation Analysis via Simple Monte Carlo Simulations," *AAS/AIAA Space Flight Mechanics Meeting*, San Diego, CA, Paper 10-134, 2010.

[6] D. Hall, S.J. Casali, L.C. Johnson, B.B. Skrehart, and L.G. Baars, "High-fidelity Collision Probabilities Estimated Using Brute Force Monte Carlo Simulations," *AAS Astrodynamics Specialist Conference*, Snowbird, UT, Paper 18-244, Aug. 2018.

[7] S. Alfano, "Orbital Covariance Interpolation," *AAS/AIAA Space Flight Mechanics Meeting*, Maui, Hawaii, Paper 04-223, Feb. 2004.

[8] D.T. Hall, M.D. Hejduk, and L.C. Johnson, "Remediating Non-Positive Definite State Covariances for Collision Probability Estimation," *AAS Astrodynamics Specialist Conference*, Columbia Valley, WA, Paper 17-567, 2017.

[9] Air Force Space Command, "Astrodynamic Standards Software," http://www.afspc.af.mil, 2018.

[10] National Research Council of the National Academies, "Continuing Kepler's Quest Assessing Air Force Space Command's Astrodynamics Standards," *The National Academies Press*, 2012.

[11] D.A. Vallado, *Fundamentals of Astrodynamics and Applications*, 2rd ed., Microcosm Press, El Segundo CA, 2001.

[12] B.D. Tapley, B.E. Schutz, and G.H. Born, *Statistical Orbit Determination*, Elsevier Academic Press, Burlington, MA, 2004.

[13] R.A. Broucke and P. J. Cefola, "On the Equinoctial Orbit Elements," *Celestial Mechanics*, Vol. 5, pp. 303-310, 1972.

[14] D. Vallado, "Covariance Transformation for Satellite Flight Dynamics Operations," *AAS/AIAA Astrodynamics Specialist Conference*, Big Sky, MT, Paper 03-526, 2003.

[15] D. Vallado and S. Alfano, "Updated Analytical Partials for Covariance Transformations and Optimization," *AAS/AIAA Space Flight Mechanics Meeting*, Williamsburg, VA, Paper 15-537, 2015.

[16] E. Anderson *et al.*, "LAPACK Users' Guide Third Edition," Society for Industrial and Applied Mathematics, Updated 22 Aug 1999 ("How to Measure Errors" at https://www.netlib.org/lapack/lug/node75.html).

[17] S.W. Shepperd, "Universal Keplerian State Transition Matrix," *Celestial Mechanics*, Vol. 35, pp. 129-144, 1985.

[18] F.L. Markley, "Approximate Cartesian State Transition Matrix," *The Journal of the Astronautical Sciences*, Vol. 34, pp. 161-169, 1986.

[19] A.P.M. Chiaradia, H.K. Kuga and A.F.B. de Almeida Prado, "Comparison between Two Methods to Calculate the Transition Matrix of Orbit Motion," *Mathematical Problems in Engineering*, Ed. M. Zanari, Vol. 2012, Article ID 768973, Hindawi Publishing Corporation, 2012.

[20] P.J. Cefola, "Equinoctial Orbit Elements – Application to Artificial Satellite Orbits," *AAS Astrodynamics Specialist Conference*, Palo Alto, CA, Paper 72-937, 1972.